Aerosol Science 40 (2009) 338 – 347

Contents lists available at ScienceDirect

Aerosol Science

journal homepage: www.elsevier.com/locate/jaerosci

# Hygroscopic growth of nucleation-mode acidic sulfate particles

G. Biskos[a,c,d], P.R. Buseck[e,f], S.T. Martin[a,b,*]

[a] School of Engineering and Applied Sciences, Harvard University, Cambridge, MA 02138, USA
[b] Department of Earth and Planetary Sciences, Harvard University, Cambridge, MA 02138, USA
[c] Department of Environmental Studies, University of the Aegean, Mytilene 81100, Greece
[d] Faculty of Applied Sciences, Delft University of Technology, Delft 2628-BL, The Netherlands
[e] School of Earth and Space Exploration, Arizona State University, Tempe, AZ 85287, USA
[f] Department of Chemistry and Biochemistry, Arizona State University, Tempe, AZ 85287, USA

ARTICLE INFO

*Article history:*
Received 26 June 2008
Received in revised form
6 December 2008
Accepted 8 December 2008

*Keywords:*
Sulfuric acid
Ammonia
Tandem DMA

ABSTRACT

The hygroscopic growth factors of acidic sulfate nanoparticles relevant to atmospheric new-particle formation and growth were measured using a tandem nano-differential mobility analyzer (TnDMA). The dry diameters of the particles ranged from 5.5 to 53.2 nm. The growth factors progressively decreased for smaller dry particle diameters. For the largest particles, a model including the Kelvin effect and assuming fully acidic particles agreed well with the observed hygroscopic growth factors. For particles having dry diameters smaller than 36.1 nm, an expanded model based on a progressively increasing extent of neutralization for smaller particles and for higher relative humidity values explained the observations. Partial neutralization occurred because of adventitious $NH_3$ in the experimental setup and was most significant for the lowest $H_2SO_4$ mass loadings, corresponding to the smallest nanoparticles. The extent of neutralization reached as high as 0.50 for the smallest particles at 80% relative humidity. Alternative explanations such as inaccuracies or nanosize effects in the density or the surface tension of the particles could not explain the observations. These results show that the hygroscopic behavior of acidic sulfate nanoparticles is more sensitive to the extent of neutralization than to the other considered possible nanosize effects, at least for dry particle diameters as small as 5.5 nm.



## 1. Introduction

Sulfuric acid, ammonia, and water are important species for the formation and subsequent growth of secondary inorganic aerosol particles in the atmosphere. For conditions that occur frequently in the atmosphere, homogeneous nucleation theory predicts that $H_2SO_4$ molecules in the gas phase form nucleation clusters with $H_2O$ and at times $NH_3$ or organic molecules (Jackervoirol & Mirabel, 1989; Kulmala, Laaksonen, & Pirjola, 1998; Pirjola & Kulmala, 1998). Field measurements provide indirect evidence in support of these predictions: the rates of new-particle formation are often higher than those estimated by considering $H_2SO_4$ and $H_2O$ molecules alone (Weber et al., 1996, 1999; Yu & Turco, 2001) yet can be reconciled in some cases by including $NH_3$ in the rate of cluster formation. The widespread occurrence of acidic sulfate particles is also supported by direct chemical composition measurements of tropospheric nanoparticles following nucleation events (Kulmala et al., 2007; Zhang et al., 2004).

* Corresponding author at: Department of Earth and Planetary Sciences, Harvard University, Cambridge, MA 02138, USA. Tel.: +1 617 495 7620; fax: +1 617 496 1471.
*E-mail addresses:* biskos@aegean.gr (G. Biskos), scot_martin@harvard.edu (S.T. Martin)
*URL:* http://www.seas.harvard.edu/environmental-chemistry (S.T. Martin).

0021-8502/$ - see front matter © 2009 Published by Elsevier Ltd.
doi:10.1016/j.jaerosci.2008.12.003

Freshly nucleated acidic sulfate particles have diameters of a few nanometers. They grow to become nucleation- and accumulation-mode particles, both by condensation of additional molecules and by coagulation with other particles. The growth rate of the nucleation-mode particles depends on their diameter, which in turn depends on relative humidity (RH). To the best of our knowledge, there are no laboratory studies of the hygroscopic growth of nucleation-mode acidic sulfate particles. The absence of data for this important chemical system can be explained at least in part by the experimental difficulty of maintaining acidic nanoparticles within an apparatus, such as the hygroscopic tandem differential mobility analyzer (DMA) used in this study. The mole-fraction-equivalent mixing ratio of monodisperse nanoparticles generated by usual laboratory methods is typically around $10^{-3}$ pptv, and $NH_3$ concentrations in an experimental system can exceed this value unless extreme care is taken. As a result, pure $H_2SO_4$ particles can fully neutralize to $(NH_4)_2SO_4$ during an experiment.

In the absence of laboratory data on acidic sulfate nanoparticles, in most applications their hygroscopic growth is predicted by using models that relate water activity to composition in conjunction with the Kelvin equation (Sarangapani & Wexler, 1996). The Kelvin effect predicts that the hygroscopic growth factors steadily decrease for particles having diameters smaller than about 50 nm (Chen, 1994; Martin, 2000). Accurate quantitative predictions of the growth factors, however, require accurate values of the surface tension and the density of the particles. Measurements of the surface tension and the density for acidic sulfate bulk solutions have been recently reported in the literature (Hyvärinen, Raatikainen, Laaksonen, Viisanen, & Lihavainen, 2005; Semmler, Luo, & Koop, 2006), but their application has not yet been tested against observations of the hygroscopic growth of acidic sulfate particles, especially those having diameters in the nano-regime.

In this work, using a tandem nano-DMA (TnDMA), we report measurements of the hygroscopic growth factors of acidic sulfate nanoparticles having theoretical dry diameters in the size range of 5.5–53.2 nm. The largest particles are nearly pure $H_2SO_4/H_2O$, but the smaller particles have a progressively higher extent of neutralization $X$ of up to 0.50. The parameter $X$ ranges from 0.0 for $H_2SO_4$ to 1.0 for $(NH_4)_2SO_4$. These highly acidic sulfate nanoparticles are similar to those that can be produced by ternary nucleation in the atmosphere.

## 2. Experimental

The tandem DMA technique (Rader & McMurry, 1986) was used for the experiments of this study. The basic apparatus (Fig. 1) is described by Biskos, Malinowski, Russell, Buseck, and Martin (2006) and Biskos, Paulsen, Russell, Buseck, and Martin (2006), and all the hygroscopic growth experiments followed the deliquescence-mode protocol described therein. Modifications were made for the study of acidified sulfate nanoparticles in a limited $NH_3$ environment. In brief, sulfuric acid aerosol nanoparticles were generated by vaporization–condensation. The polydisperse $H_2SO_4/H_2O$ particles were passed through a $^{210}Po$ bipolar charger (NRD Model P-2031) and a first nano-DMA (TSI Model 3085) (DMA-1) to extract a monodisperse sample. Ultrahigh purity (UHP) $N_2$, passed through a citric acid filter to remove $NH_3$, was used as the sheath flow for DMA-1. The monodisperse particles exiting DMA-1 were at low RH and composed of concentrated sulfuric acid of acid weight percent $w_t^1$. In the main experimental configuration (Fig. 1a), the monodisperse particles were then conditioned inside a single Nafion tube humidity exchanger (Perma Pure Model MD-110) to a higher RH, corresponding to a solution having a solute weight percent $w_t$. The RH history of the sample was therefore (< 5%) → ($xx$%), where $xx$ was increased stepwise as the independent variable of the hygroscopic growth measurements.

In addition to $H_2O$ uptake, some absorption of adventitious $NH_3$, even with the presence of scrubbers, also occurred inside the Nafion tube humidity exchanger. Both $H_2O$ and $NH_3$ in the outer annulus of the tube passed through the Nafion membrane into the inner annulus where the aerosol flowed. The Nafion membrane also absorbed $NH_3$ and released it slowly at later times. The release rate was enhanced at higher RH. The extent of partial neutralization from these processes, yielding acidic $(NH_4)_{2X}H_{2(1-X)}SO_4/H_2O$ particles, was increasingly significant for the lowest $H_2SO_4$ mass loadings (corresponding to the smallest particle diameters) and the highest RH conditions. By changing the extent of neutralization, the $NH_3$ absorption indirectly affected particle $H_2O$ uptake.

The size distribution of the acidic $(NH_4)_{2X}H_{2(1-X)}SO_4/H_2O$ particles exiting the humidity exchanger was measured with a second nano-DMA (DMA-2) and an ultrafine condensation particle counter (CPC, TSI Model 3025). Calibration of the system, as described in Biskos, Paulsen et al. (2006), was performed prior to the experiments, leading to a precision between selected and measured diameters of the dry monodisperse particles of better than 1%. DMA-2 used a recirculating loop for the sheath flow, for which all stainless steel piping was used to avoid potential contaminants (Middlebrook, Thomson, & Murphy, 1997).

In an alternative configuration (Fig. 1b), the $H_2SO_4/H_2O$ particles exiting DMA-1 were exposed to a 0.01 Lpm $NH_3$(g) flow instead of passing through the Nafion tube, and the size change resulting from conversion from aqueous $H_2SO_4/H_2O$ droplets to solid $(NH_4)_2SO_4$ particles was measured with DMA-2. A conceptual cartoon of the principle for these experiments is depicted in Fig. 2. For these measurements, the Nafion tube humidity exchanger between the two DMAs was replaced with stainless steel tubing, $NH_3$(g) was introduced between DMA-1 and DMA-2, and an open sheath flow system was employed in DMA-2 (cf. comparison of Fig. 1a with Fig. 1b).

Additional information regarding both configurations (Fig. 1a and b) is as follows. UHP concentrated sulfuric acid (Sigma Aldrich, 99.999% on metals assay basis) was used in the vaporization–condensation aerosol generator. The acid was placed in a glass U-tube of 20-mm inner diameter without filling the tube, thereby forming a bath over which UHP nitrogen gas flowed at 1 Lpm. Aerosol particles formed downstream in a subsequent cooling section, which was set at either 0 °C or ambient. The mean diameter and the number concentration of the particles were controlled by adjusting the temperature difference between the

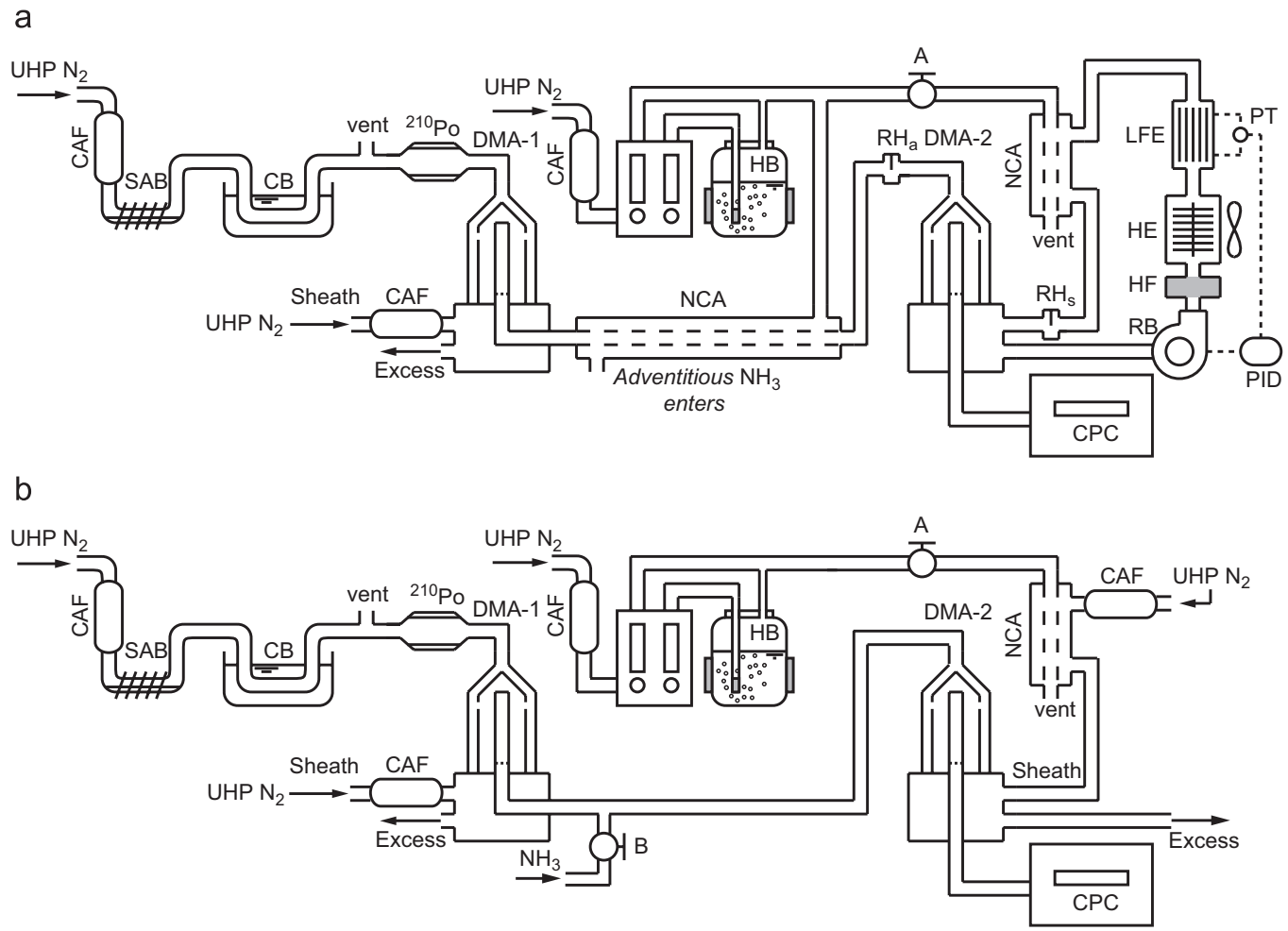


**Fig. 1.** Schematic layout of the tandem nano-DMA (TnDMA) setup used for (a) the measurement of the hygroscopic growth factor of monodisperse acidic sulfate nanoparticles and (b) the determination of the weight percent acid content based on the diameter change upon $NH_3$ exchange for $H_2O$ (cf. Fig. 2). Key: UHP, ultrahigh purity; CAF, citric acid filter; SAB, sulfuric acid bath; CB, cooling bath; HB, humidifying bubbler; $^{210}Po$, polonium source bipolar charger; NCA, Nafion conditioner with air (humidity exchanger); DMA, differential mobility analyzer; CPC, condensation particle counter; RB, recirculation blower; HF, high efficiency particulate air (HEPA) filter; HE, heat exchanger; PT, pressure transducer; PID, proportional-integral-derivative controller; LFE, laminar flow element; $RH_a$, aerosol-flow relative-humidity monitor of DMA-2; and $RH_s$, sheath-flow relative-humidity monitor of DMA-2. Valve A is adjusted during the hygroscopic growth experiments to equalize the RH of the aerosol and sheath flows. For the determination of the acid content in setup b, NCA is replaced by a stainless steel pipe, and valve B serves as an inlet for $NH_3$. 0.01 Lpm of $NH_3$ is mixed with the 0.3 Lpm of monodisperse aerosol.

heated acid bath (60–100 °C) and the cooling section. As an example, when the $H_2SO_4$ bath was maintained at 100 °C and the cooling section was at ambient temperature, the aerosol particles had a mode diameter of 40 nm, a geometric standard deviation (gsd) of 1.32, and an integrated number concentration of $7 \times 10^6$ particles $cm^{-3}$. When the respective temperatures were 60 and 0 °C, the respective values of these quantities were 13 nm, 1.3, and $3 \times 10^6$ particles $cm^{-3}$. The polydisperse nanoparticles were carried through glass and stainless steel tubing to the bipolar charger and DMA-1.

With regard to adventitious $NH_3$, the ubiquity of ammonia in the atmosphere causes difficulties for the study of acid aerosol nanoparticles in the laboratory. Typical outdoor concentrations of $NH_3$ range from 0.1 to 10 ppb (Seinfeld & Pandis, 1998), and indoor concentrations are often an order of magnitude higher (e.g., Leaderer et al., 1999; Suh, Koutrakis, & Spengler, 1994). Furthermore, the 99.999% purity of the $N_2$ used in the experiments implies impurities of up to $10^4$ ppbv, a fraction of which is $NH_3$. In comparison, after monodisperse size selection, the sulfate particle mass loadings in our experiments correspond to $2.8 \times 10^{-6}$ ppbv for the smallest particles to 1.1 ppbv for the largest particles.

Careful attention was given to minimizing all sources of $NH_3$(g) in the TnDMA. The $N_2$ carrier gas flows of the polydisperse aerosol, the sheath air in DMA-1, and of the purge air in the Nafion tubes were all passed through $NH_3$ scrubbers, which consisted of cylindrical 400 $cm^3$ containers filled with granular citric acid (J. T. Baker, 100% purity). For further minimization of $NH_3$ infiltration, the water used in the bubbler to humidify the purge flows in the Nafion tubes was renewed daily. It was also transported from the Millipore system (Barnstead Model D8971; 18MΩ cm) to the water bubbler of the TnDMA without exposure to laboratory air through use of a sealed flask, which had been purged with $NH_3$-scrubbed UHP $N_2$ before use. In addition, high concentrations of $H_2SO_4$ particles were passed through the TnDMA for ca. 30 min before every measurement to scavenge $NH_3$

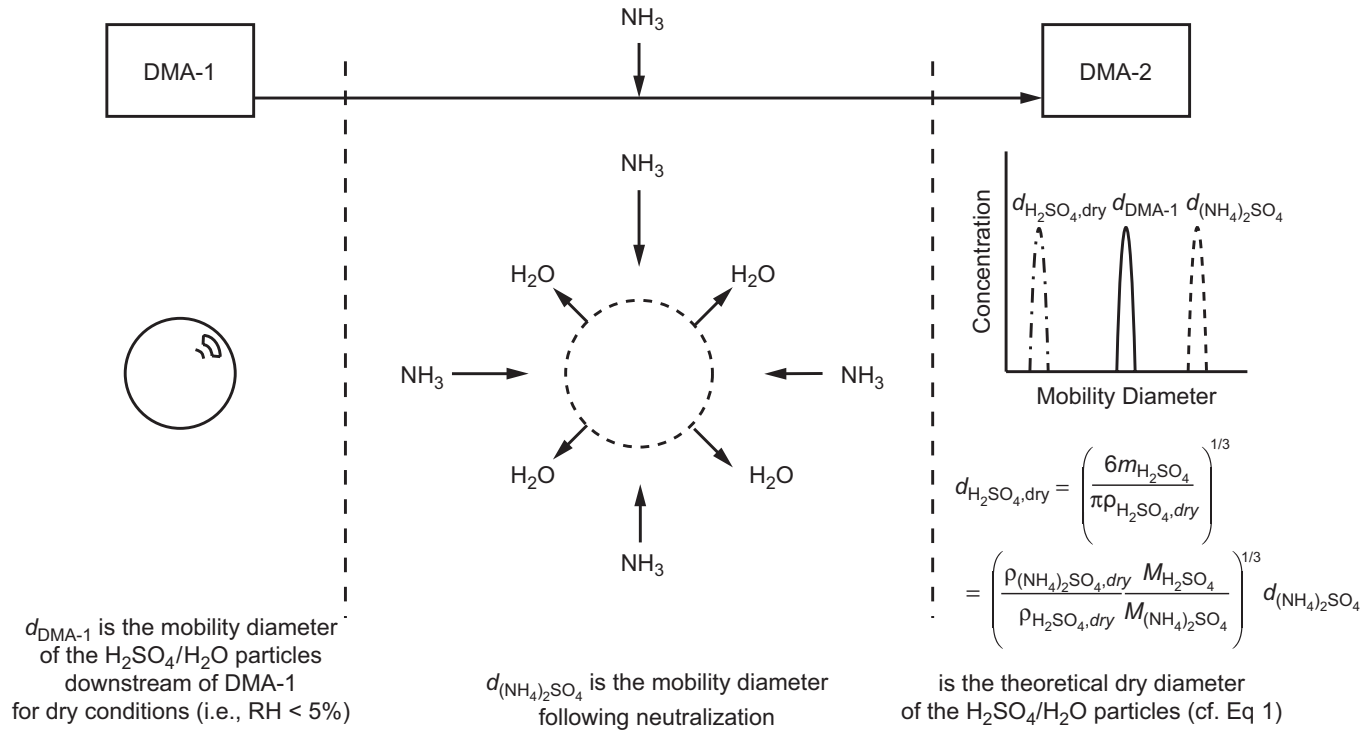


**Fig. 2.** Explanatory cartoon of the experimental design for determining the acid content of the sulfuric acid nanoparticles by the principle of $NH_3$ exchange for $H_2O$. Monodisperse $H_2SO_4/H_2O$ particles downstream of DMA-1 are exposed to high concentrations of $NH_3$ gas, and the resulting size change is recorded by DMA-2 and the ultrafine CPC. The particle-size change results from exchange of $NH_3$ for $H_2O$. The sulfate mass deduced from the diameter of the solid $(NH_4)_2SO_4$ particles is used to calculate the theoretical dry diameter $d_{H_2SO_4,dry}$ (i.e., RH = 0%) of $H_2SO_4$ particles by Eq. (1) and to calculate the acid content $w_t^1$ of $H_2SO_4/H_2O$ particles in DMA-1 by Eq. (2). Although the cartoon depicts an increase in diameter upon neutralization, a decrease in diameter is also possible depending on the original acid content (cf. Eq. (3)).

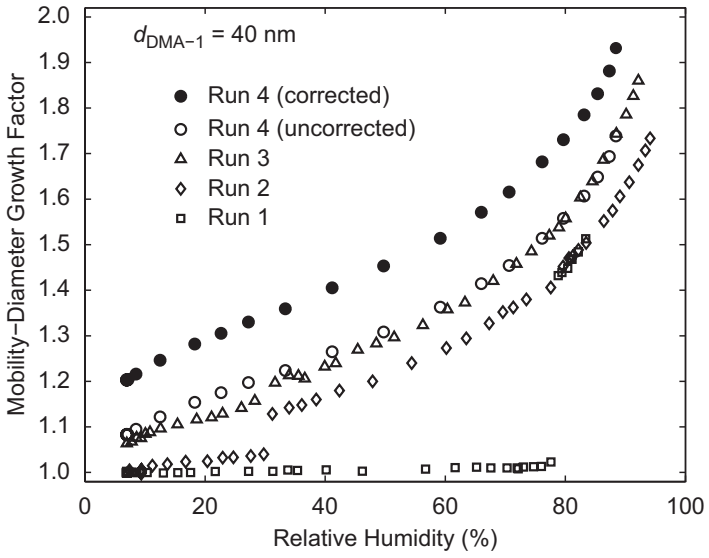


**Fig. 3.** Hygroscopic growth measurements of acidic sulfate particles corresponding to runs that have progressively less adventitious $NH_3$(g) present in the TnDMA system represented by Fig. 1a. Except for the corrected run 4, the hygroscopic growth factor in this figure is taken as $d_{DMA-2}/d_{DMA-1}$. The correction for run 4 is the adjustment of $d_{DMA-1}$ for water content based on $NH_3$ exchange, giving the quantity $d_{H_2SO_4,dry}$ for use in the denominator of the growth-factor calculation (cf. Fig. 2 and Eq. (4a)). Run 1: unscrubbed UHP $N_2$ was used for the $H_2SO_4$ nanoparticle generator and house compressed air for the remainder of the system. Run 2: unscrubbed UHP $N_2$ was used for all flows in the system, including in the $H_2SO_4$ nanoparticle generator, in the sheath flow in DMA-1, and in the purge air of the Nafion tube conditioners. Run 3: UHP $N_2$ with citric-acid $NH_3$ scrubbers was used for the $H_2SO_4$ nanoparticle generator and for the sheath flow in DMA-1. Run 4: as run 3 except that $NH_3$-scrubbed air was also used in the purge air of the Nafion tube conditioners. The water in the bubbler was renewed daily.

that desorbed from the inner walls of the apparatus and other locations. With these procedures, we maintained the extent of neutralization in the acidic regime for all experiments, including those with the smallest mass loadings (i.e., smallest particle sizes).

Fig. 3 shows the results of early measurements as examples of the importance of the $NH_3$ scrubbing. When unscrubbed UHP $N_2$ was used through the $H_2SO_4$ nanoparticle generator, along with house compressed air for the sheath flow in DMA-1, particles having nominal diameters (i.e., diameters determined by the settings in DMA-1) of 40 and 60 nm had hygroscopic responses, including deliquescence and growth, of ammonium sulfate. Example results are shown as run 1 in Fig. 3. Subsequent use of UHP $N_2$ for the sheath flow without any $NH_3$ scrubbers in DMA-1 (run 2 of Fig. 3) significantly increased the acidity of the particles, although discontinuities in the growth curve were still observed at intermediate RH values. The discontinuities indicated the occurrence of phase transitions and therefore implied $X > 0.5$. Use of UHP $N_2$ with $NH_3$ scrubbers throughout the system except for the Nafion exchangers resulted in even higher acidity levels, as indicated by higher hygroscopic growth of the particles. Even so, the small discontinuities in the growth curve indicated partial neutralization of the particles (run 3). Further use of the in-line $NH_3$ scrubbers for the Nafion exchangers, in conjunction with additional frequent renewal of the water in the bubbler, resulted in even higher acidity levels, as indicated by the continuous growth curve (run 4).

## 3. Results and discussion

### 3.1. Acid content of the sulfuric acid nanoparticles at low relative humidity

Determination of the acid content of the particles exiting DMA-1 and their associated theoretical dry diameter $d_{H_2SO_4,dry}$ is necessary for the measurement of a meaningful hygroscopic growth factor using the TnDMA (cf. denominator of Eq. (4a)). Although the RH over concentrated sulfuric acid solutions is negligible, there is an enrichment process in the water content of the aerosol particles generated by vaporization–condensation. The vapor pressure of $H_2O$ is greater than that of $H_2SO_4$ over concentrated sulfuric acid (95–98 wt%) because the azeotrope occurs at ca. 98.5 wt% (Gmitro & Vermeulen, 1964). For an acid bath between 95 and 98 wt%, the corresponding vapor is 72–92 wt% acid, with only a small dependence on temperature between 60 and 100 °C (Mudd, Kruger, & Murray, 1982). Particle compositions should therefore lie within this same wt% range, omitting differential loss of the two species to the walls. In principle, measurement of the RH indicates the wt% composition of the droplet in the absence of a Kelvin effect. The RH values corresponding to 72 to 92 wt% acid are, however, below 5%. Typical RH sensors, including ours, are not capable of accurately measuring RH values below 5%.

A separate set of experiments based on the diameter change with $NH_3$ neutralization (setup of Fig. 1b) was conducted to infer the acid content of the initial $H_2SO_4$ particles. Monodisperse sulfuric acid particles of $X = 0$ exiting DMA-1 were fully neutralized to $X = 1$ by exposure to high concentrations of $NH_3$(g) from a cylinder of anhydrous $NH_3$ (McMurry, Takano, & Anderson, 1983). The diameter after neutralization, corresponding to crystallized $(NH_4)_2SO_4$ particles, was measured using DMA-2 and the ultrafine CPC. The diameter and the density of the $(NH_4)_2SO_4$ particles yielded the sulfate mass in the particles, from which the corresponding theoretical dry diameters of the pure $H_2SO_4$ particles were estimated (cf. Fig. 2). Particles of all diameters had $X = 0$ before the aerosol was mixed with $NH_3$ because the RH-adjusting Nafion tube was omitted.

Fig. 4 shows the results of the acid-content experiments for particles having nominal diameters $d_{DMA-1}$ from 10 to 60 nm. The experimental data are expressed as growth factors, calculated as the diameter measured by DMA-2 relative to the diameter set by DMA-1 (based on the adjusted voltage and the sheath flow rate). Measurements 1a to 3a correspond to the mean mobility

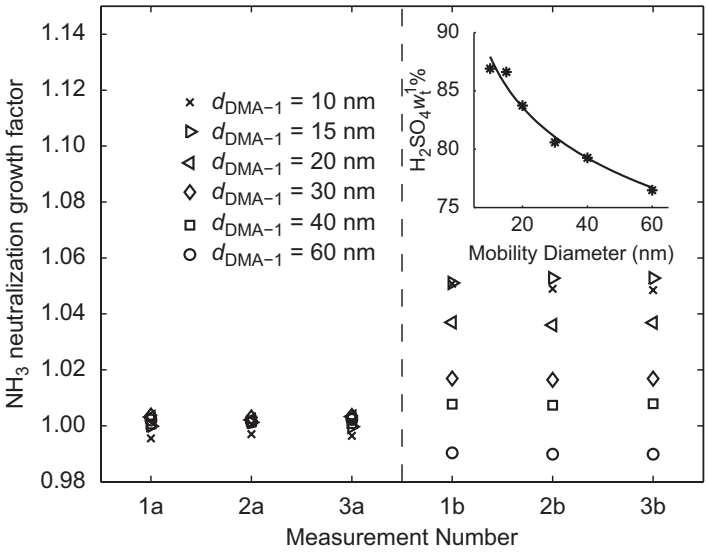


**Fig. 4.** Size changes arising from $NH_3$ exchange for $H_2O$ in the $H_2SO_4$ particles, corresponding to the experimental setup of Fig. 1b. Results are expressed as the $NH_3$-neutralization growth factor $\mathbf{g_{NH_3}}$. Measurement sets *a* and *b* correspond, respectively, to $H_2SO_4/H_2O$ and $(NH_4)_2SO_4$ particles (i.e., particles before and after exposure to high concentrations of $NH_3$ gas). Measurements 1, 2, and 3 show reproducibility of results for identical experiments.

**Table 1**
Results for $d_{H_2SO_4,dry}$ (nm) and $w_t^1$ (%) based on measurements of $\boldsymbol{d}_{\mathbf{H_2SO_4}}(\boldsymbol{w_t^1})$ and $\boldsymbol{d}_{\mathbf{(NH_4)_2SO_4}}$ and application of Eqs. (1) and (2c).

| $d_{DMA\text{-}1}$[a] | $\boldsymbol{d}_{\mathbf{H_2SO_4}}(\boldsymbol{w_t^1})$[b] | $\boldsymbol{d}_{\mathbf{(NH_4)_2SO_4}}$[c] | $d_{H_2SO_4,dry}$[d] | $w_t^1$[e] |
|---|---|---|---|---|
| 6.0 | n/a | n/a | 5.5[f] | n/a |
| 8.0 | n/a | n/a | 7.5[f] | n/a |
| 10.0 | 9.97 | 10.5 | 9.4 | 86.9 |
| 15.0 | 15.01 | 15.8 | 14.1 | 86.6 |
| 20.0 | 20.05 | 20.7 | 18.6 | 83.7 |
| 30.0 | 30.10 | 30.5 | 27.3 | 80.6 |
| 40.0 | 40.05 | 40.3 | 36.1 | 79.2 |
| 60.0 | 60.10 | 59.4 | 53.2 | 76.5 |

[a]Nominal diameter dialed by DMA-1.

[b]Diameter measured by DMA-2 before $NH_3$ substitution for $H_2O$ (i.e., valve B closed). Uncertainty is less than 1%. Relative humidity is below sensor capability (i.e., RH < 5%).

[c]Diameter measured by DMA-2 after $NH_3$ substitution for $H_2O$ (i.e., with valve B open). Uncertainty is less than 1%.

[d]Theoretical dry diameter calculated by Eq. (1). The propagated uncertainty is less than 1%.

[e]Acid weight percent calculated by Eq. (2c). The propagated uncertainty is less than 3%.

[f]Extrapolated from results for larger diameters.

diameters of the $H_2SO_4/H_2O$ particles before exposure to high concentrations of $NH_3$ gas (i.e., valve B closed). The results show the reproducibility of the experimental setup and the particle generation conditions on various days. Small deviations from unity for 1a to 3a reflect the measurement uncertainty (< 1%) in the operation of the two DMAs after calibration (Biskos, Paulsen et al., 2006; Kim, Mulholland, Kukuck, & Pui, 2005). The reproducibility is especially important because the neutralization and hygroscopic growth experiments were carried out on different days between thorough instrument cleaning and venting as needed for rigorous exclusion of $NH_3$.

Measurements 1b to 3b show the growth factors following neutralization when valve B was opened. Particles having nominal $d_{DMA-1}$ of 60 nm shrink, whereas those under 40 nm grow. The diameter change, which depends on the number of water molecules replaced by $NH_3$ in the original $H_2SO_4/H_2O$ droplets, provides a measurement of their acid content.

The equations for determining the acid content using this method are developed as follows. The theoretical diameter of anhydrous sulfuric acid $d_{H_2SO_4,dry}$ at 0% RH is related to the diameter of the neutralized particles $\boldsymbol{d}_{\mathbf{(NH_4)_2SO_4}}$ measured by DMA-2 as follows:

$$d_{H_2SO_4,dry} = \left(\frac{6m_{H_2SO_4}}{\pi\rho_{H_2SO_4,dry}}\right)^{1/3} = \left(\frac{\rho_{(NH_4)_2SO_4,dry}}{\rho_{H_2SO_4,dry}}\frac{M_{H_2SO_4}}{M_{(NH_4)_2SO_4}}\right)^{1/3}\boldsymbol{d}_{\mathbf{(NH_4)_2SO_4}}, \tag{1}$$

where $\rho$ is density, $M$ is molecular weight, and $m_{H_2SO_4}$ is the mass of $H_2SO_4$ in the unneutralized monodisperse particles. Bold quantities in Eq. (1) and elsewhere represent those measured by us using the experimental setup. The uncertainty of the terms in the cube-root of Eq. (1) is small so that the uncertainty of $d_{H_2SO_4,dry}$ is that of the measurement of $\boldsymbol{d}_{\mathbf{(NH_4)_2SO_4}}$ (i.e., within less than 3%). The acid content in the unneutralized particles exiting DMA-1, expressed in weight percent $w_t^1$, is determined from the diameter $\boldsymbol{d}_{\mathbf{H_2SO_4}}(\boldsymbol{w_t^1})$ corresponding to the selected diameter by DMA-1 through the solution of Eq. (2c):

$$w_t^1 = 100\frac{\rho_{H_2SO_4,dry}}{\rho_{H_2SO_4}(w_t^1)}\left(\frac{d_{H_2SO_4,dry}}{\boldsymbol{d}_{\mathbf{H_2SO_4}}(\boldsymbol{w_t^1})}\right)^3 \tag{2a}$$

$$= 100\frac{\rho_{(NH_4)_2SO_4,dry}}{\rho_{H_2SO_4}(w_t^1)}\frac{M_{H_2SO_4}}{M_{(NH_4)_2SO_4}}\left(\frac{\boldsymbol{d}_{\mathbf{(NH_4)_2SO_4}}}{\boldsymbol{d}_{\mathbf{H_2SO_4}}(\boldsymbol{w_t^1})}\right)^3 \tag{2b}$$

$$= 100\frac{\rho_{(NH_4)_2SO_4,dry}}{\rho_{H_2SO_4}(w_t^1)}\frac{M_{H_2SO_4}}{M_{(NH_4)_2SO_4}}\boldsymbol{g}_{\mathbf{NH_3}}^3, \tag{2c}$$

where $\boldsymbol{g}_{\mathbf{NH_3}}$ is the $NH_3$-neutralization growth factor. The equation for the density of the $H_2SO_4/H_2O$ particles is given in Table S1.

For the experiments performed, Table 1 lists the nominal diameter $d_{DMA-1}$, the measured diameters $\boldsymbol{d}_{\mathbf{H_2SO_4}}(\boldsymbol{w_t^1})$ and $\boldsymbol{d}_{\mathbf{(NH_4)_2SO_4}}$, and the calculated diameter $d_{H_2SO_4,dry}$ and acid weight percent $w_t^1$. The theoretical dry diameters of the 6- and 8-nm particles were extrapolated from this data set because the particle number concentrations following dilution with $NH_3$(g) were too low for accurate measurement of the change in diameter upon neutralization. The good agreement between $d_{DMA-1}$ and $\boldsymbol{d}_{\mathbf{H_2SO_4}}(\boldsymbol{w_t^1})$ in the experimental configuration of Fig. 1b further implicates the importance of the Nafion tube as the entry point of adventitious $NH_3$ and $H_2O$ in the configuration of Fig. 1a, even for the lowest RH values.

The inset of Fig. 4 shows the size dependence determined for the acid content of the particles. Smaller particles had higher acid contents. For particles having $d_{DMA-1}$ of 10 nm, the weight percent of acid was 86.9%. The acid content for 60-nm particles was 76.5%. The progressive increase in acid content for decreasing particle size can be explained by the greater importance of the Kelvin effect for the smaller particles.

The size change upon neutralization follows from Eqs. (1) and (2a) as follows:

$$\delta d_{neutralization} = \boldsymbol{d}_{(\mathbf{NH_4})_2\mathbf{SO_4}} - \boldsymbol{d}_{\mathbf{H_2SO_4}}(\boldsymbol{w}_t^1) \tag{3a}$$

$$= \left[ \left( \frac{\rho_{H_2SO_4,dry}}{\rho_{(NH_4)_2SO_4,dry}} \frac{M_{(NH_4)_2SO_4}}{M_{H_2SO_4}} \right)^{1/3} - \left( \frac{100}{w_t^1} \frac{\rho_{H_2SO_4,dry}}{\rho_{H_2SO_4}(w_t^1)} \right)^{1/3} \right] d_{H_2SO_4,dry}. \tag{3b}$$

An increase or decrease in diameter upon neutralization is governed by the sign of the term in the brackets, corresponding, respectively, to an $NH_3$-neutralization growth factor above or below unity. Based on the parameters in Table S1, this term is positive, indicating that the diameter increases upon neutralization, for $w_t^1 > 78.2\%$. This value is approximate because, among other factors, the density equation in Table S1 is calibrated only to 70 wt%, and thus extrapolation is required. The inference from the data of Fig. 4 is that particles having nominal diameters $d_{DMA-1}$ of ca. 45 nm and smaller have an acid weight percent composition greater than 78.2% and therefore grow larger when neutralized by $NH_3$.

### 3.2. Hygroscopic growth experiments

The TnDMA was used to measure the hygroscopic growth of the acidic $(NH_4)_{2X}H_{2(1-X)}SO_4/H_2O$ nanoparticles (setup of Fig. 1a). The observable in the growth experiments is the mobility diameter $d_m$ of the particles. Liquid droplets such as the acidified sulfate particles of this study are spherical, so the mobility diameter and the volume-equivalent diameter are equal. In this case, the mobility-diameter growth factor $g$ and the diameter growth factor are equivalent and are given by:

$$g^{meas}(\mathbf{RH}) = \frac{d_m(\mathbf{RH})}{d_{m,dry}} = \frac{\boldsymbol{d}_{(\mathbf{NH_4})_{2X}\mathbf{H}_{2(1-X)}\mathbf{SO_4}}(\mathbf{RH})}{d_{H_2SO_4,dry}} \tag{4a}$$

$$= \left( \frac{\rho_{H_2SO_4,dry}}{\rho_{(NH_4)_2SO_4,dry}} \frac{M_{(NH_4)_2SO_4}}{M_{H_2SO_4}} \right)^{1/3} \left( \frac{\boldsymbol{d}_{(\mathbf{NH_4})_{2X}\mathbf{H}_{2(1-X)}\mathbf{SO_4}}(\mathbf{RH})}{\boldsymbol{d}_{(\mathbf{NH_4})_2\mathbf{SO_4}}} \right), \tag{4b}$$

where $\boldsymbol{d}_{(\mathbf{NH_4})_{2X}\mathbf{H}_{2(1-X)}\mathbf{SO_4}}(\mathbf{RH})$ is the diameter measured by DMA-2 following hygroscopic growth. The uncertainty in $g^{meas}$ is within 3% based on error propagation using Eq. (4b). Eq. (4b) corrects for the water content of the $H_2SO_4/H_2O$ particles, thereby providing a growth factor normalized to a notional 100% acid content. Xiong, Zhong, Fang, Chen, and Lippmann (1998) provided a similar definition for a growth factor for pure $H_2SO_4/H_2O$ particles, although that study did so as a fitting factor to measurements rather than as an independent measurement of acid content as done herein. The 100% acid content is notional because anhydrous $H_2SO_4$ decomposes into $SO_3$ and other species.

The measured hygroscopic growth factors of particles having theoretical dry diameters $d_{H_2SO_4,dry}$ from 5.5 to 53.2 nm are shown in Fig. 5. For fixed RH, the hygroscopic growth of the particles decreases with decreasing particle size. For example, the measured growth factor at 81% RH is 1.40 for the smallest particles compared to 1.80 for the largest particles. For comparison, the respective values for analogous diameters are 1.22 and 1.44 for $(NH_4)_2SO_4$ particles and 1.51 and 1.77 for NaCl particles (Biskos, Paulsen et al., 2006; Biskos, Russell, Buseck, & Martin, 2006). The largest particles (i.e., 60-nm nominal diameter) are thus more hygroscopic than both $(NH_4)_2SO_4$ and NaCl particles of similar size. This result is expected because $H_2SO_4$ is a more hygroscopic material. The Kelvin effect is also small for this diameter so that differences in surface tension are not as important.

In comparison, although the smallest particles (i.e., 6-nm nominal diameter) are more hygroscopic than $(NH_4)_2SO_4$ particles of similar size, they are less so than NaCl particles. Assuming pure $H_2SO_4/H_2O$ particles, this shift in relative growth factors cannot be explained by a differential Kelvin effect. On the contrary, an increase in the relative growth factor is expected for $H_2SO_4/H_2O$ compared to $(NH_4)_2SO_4/H_2O$ and $NaCl/H_2O$ nanoparticles because of the smaller surface tension of $H_2SO_4/H_2O$ (Hyvärinen et al., 2005). The modeling analysis that follows below provides evidence that the relative hygroscopicity of the smallest particles falls off because of partial neutralization. Water uptake decreases monotonically for increasing neutralization from $X = 0.0$ to 0.50, as plotted in the inset in the panel for 53.2-nm dry particles in Fig. 5.

For pure $H_2SO_4/H_2O$ particles (i.e., $X = 0$), the modeled hygroscopic growth factor $g^{model}(a_w)$ is as follows:

$$g^{model}(a_w) = \left( \frac{100}{w_t(a_w)} \frac{\rho_{H_2SO_4,dry}}{\rho_{H_2SO_4}(w_t(a_w))} \right)^{1/3}, \tag{5}$$

where $a_w$ is the water activity. The term $w_t$ is the acid weight percent after passing through the Nafion tube humidity exchanger and coming to equilibrium with the elevated RH. The model analysis considers a case for a growth factor $g_{bulk}^{model}(\mathrm{RH})$ that omits the Kelvin effect by assuming that $a_w = \mathrm{RH}/100$. The dotted lines in Fig. 5 show $g_{bulk}^{model}(\mathrm{RH})$ based on the properties listed in Table S1 for $H_2SO_4/H_2O$. As evident in Fig. 5, the model does not adequately explain the observations for any particle size.

The model analysis considers another case for a growth factor $g_{Kelvin}^{model}(\mathrm{RH})$ that accounts for the Kelvin effect by relating RH to $a_w$ as follows:

$$\mathrm{RH} = 100 a_w \exp\left( \frac{4 M_w \sigma_{H_2SO_4}(w_t(a_w))}{RT \rho_w d_{H_2SO_4}(a_w)} \right), \tag{6}$$

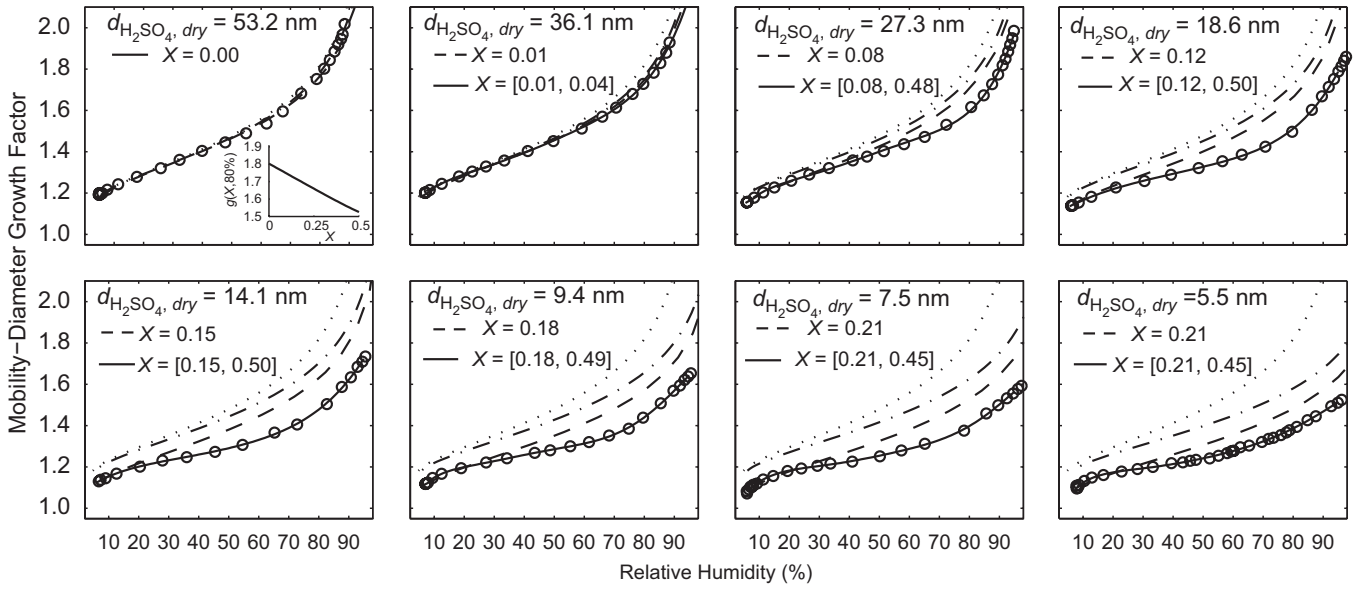


**Fig. 5.** Hygroscopic growth factors of acidic sulfate nanoparticles having theoretical dry diameters $d_{H_2SO_4,dry}$ of 5.5–53.2 nm. The growth factors are based on Eq. (4b). The lines show the modeled growth factors for (a) $H_2SO_4/H_2O$ particles without a Kelvin effect (dotted lines), (b) $H_2SO_4/H_2O$ particles with a Kelvin effect (dash-dotted lines), (c) acidic $(NH_4)_{2X}H_{2(1-X)}SO_4/H_2O$ particles with a Kelvin effect and having an invariant extent of neutralization $X$ optimized to fit the data at low RH (dashed lines), and (d) acidic $(NH_4)_{2X}H_{2(1-X)}SO_4/H_2O$ particles with a Kelvin effect and having an RH-dependent extent of neutralization (cf. Eqs. (5)–(8)) (solid lines). For the final model case, the range of the extent of neutralization $X$ is indicated in each panel in brackets, and the extent of neutralization increases monotonically for low to high RH (not shown).

where $\rho_w$ is the density of pure water, $M_w$ is the molar mass of water, $\sigma_{H_2SO_4}(w_t(a_w))$ is the surface tension of the $H_2SO_4/H_2O$ (Table S1), $R$ is the universal gas constant, and $T$ is the temperature. By definition, we also have that $d_{H_2SO_4}(a_w) = g^{model}(a_w)d_{H_2SO_4,dry}$. The dash-dotted lines in Fig. 5 represent the case of $g^{model}_{Kelvin}$ (RH), which is evaluated as a parametric plot of $g^{model}(a_w)$ of Eq. (5) vs. RH($a_w$) of Eq. (6) with the common variable $a_w$. There is excellent agreement between $g^{meas}$ (RH) and $g^{model}_{Kelvin}$ (RH) for the particles having a theoretical dry diameter of 53.2 nm.

As mentioned above, the growth factors intermediate to $(NH_4)_2SO_4$ and NaCl for the smallest particle sizes imply partial neutralization. For particles with theoretical dry diameters of 36.1 nm and smaller, predictions of growth factors for partially neutralized particles are also included in Fig. 5 (dashed lines) for extents of neutralization optimized to fit the low RH data at each particle diameter. The equation for the hygroscopic growth factor in this case is as follows:

$$g^{model}_{(NH_4)_{2X}H_{2(1-X)}SO_4}(a_w;X) = \frac{d_{(NH_4)_{2X}H_{2(1-X)}SO_4}(a_w;X)}{d_{H_2SO_4,dry}} \tag{7a}$$

$$= \left(\frac{100}{w_t(a_w;X)}\frac{\rho_{(NH_4)_{2X}H_{2(1-X)SO_4,dry}}}{\rho_{(NH_4)_{2X}H_{2(1-X)}SO_4}(w_t(a_w;X);X)}\right)^{1/3}\frac{d_{(NH_4)_{2X}H_{2(1-X)}SO_4}(X)}{d_{H_2SO_4,dry}} \tag{7b}$$

$$= \left(\frac{100}{w_t(a_w;X)}\frac{\rho_{H_2SO_4,dry}}{\rho_{(NH_4)_{2X}H_{2(1-X)}SO_4}(w_t(a_w;X);X)}\frac{M_{(NH_4)_{2X}H_{2(1-X)}SO_4}}{M_{H_2SO_4}}\right)^{1/3}, \tag{7c}$$

using $d_{(NH_4)_{2X}H_{2(1-X)}SO_4,dry}(X) = ((\rho_{H_2SO_4,dry}/\rho_{(NH_4)_{2X}H_{2(1-X)}SO_4,dry})(M_{(NH_4)_{2X}H_{2(1-X)}SO_4}/M_{H_2SO_4}))^{1/3}d_{H_2SO_4,dry}$. The value $d_{H_2SO_4,dry}$ appears in the denominator of Eq. (7a) because partial neutralization occurs only after DMA-1. The equation including the Kelvin effect for the partially neutralized particles is as follows:

$$\mathrm{RH} = 100a_w \exp\left(\frac{4M_w\sigma_{(NH_4)_{2X}H_{2(1-X)}SO_4}(w_t(a_w;X);X)}{RT\rho_w d_{(NH_4)_{2X}H_{2(1-X)}SO_4}(a_w;X)}\right). \tag{8}$$

The term $w_t$ in Eqs. (7) and (8) represents the weight percent of $(NH_4)_{2X}H_{2(1-X)}SO_4$ in the droplet, with the balance from water. The dashed lines in Fig. 5 show Eqs. (7c) and (8) plotted parametrically in $a_w$ for $X$ values of 0.01 (36.1 nm), 0.08 (27.3 nm), 0.12 (18.6 nm), 0.15 (14.1 nm), 0.18 (9.4 nm), 0.21 (7.5 nm), and 0.21 (5.5 nm). The extent of neutralization increases for smaller particle sizes because of the correspondingly lower $H_2SO_4$ mass loadings in the system.

The RH-independent $X$ values decrease the predicted growth factors sufficiently to bring measurements and model predictions into agreement at low RH. However, the modeled growth factors remain too high for elevated RH. The implication is that neutralization increases for increasing RH. The solid lines in Fig. 5 show the model of Eqs. (7c) and (8) for which an RH-dependent

extent of neutralization $X$(RH) is optimized to fit the observations. The range of $X$(RH) for each particle diameter is indicated in each panel in brackets. The extent of neutralization increases monotonically and smoothly from low to high RH (not shown). The greater neutralization with increasing RH results both from the faster release rate of $NH_3$ absorbed in the Nafion and the greater permeability of Nafion to $NH_3$ from the outer to inner annulus of the conditioner.

Two interesting trends are apparent for $X$ among the panels in Fig. 5. The first is that a large jump occurs in $X$ for particles having a theoretical dry diameter of 36.1 nm compared to those of 27.3 nm. For example, $X$(90%) shifts from 0.04 to 0.48. The explanation is that the temperature in the particle generation method was switched from ambient to 0 °C in the cooling section between these compositions, leading to a drastic reduction in particle concentration and hence total sulfuric acid mixing ratio. For similar amounts of total $NH_3$ between the two experiments, greater neutralization occurs for the lower sulfuric acid mixing ratio.

The second trend is the relative consistency in $X$ among particles having $d_{H_2SO_4,dry}$ of 27.3 nm and smaller. For example, $X$(90%) varies within 0.45–0.50 for the six experiments from 5.5 to 27.3 nm. Reasonable assumptions when comparing these experiments are that the total available $NH_3$ does not vary greatly and that total $H_2SO_4$ decreases for smaller particle sizes. The follow-on thought is that, all other factors being equal, partial neutralization of largest particles implies full neutralization of the smallest particles, contrary to the observations shown in Fig. 5. Growth rate kinetics, however, can provide an explanation of the observations. In the kinetic regime of high Knudsen numbers applicable to nanoparticles at 1 atm, the molar flow $J$ (moles $s^{-1}$) by uptake of gas-phase molecules into the particles scales in proportion to particle surface area. Smaller particles in the fixed residence time in the Nafion tube take up fewer moles of $NH_3$, albeit those moles are diluted in smaller volumes. The higher $NH_3$ vapor pressures because of the Kelvin effect further slows the growth rates of the smaller compared to the larger particles. These compensating factors may explain the consistency of $X$(90%) for the particles having $d_{H_2SO_4,dry}$ of 27.3 nm and smaller.

The evaluations of Eqs. (7c) and (8) shown in Fig. 5 requires use of terms depending on $X$, including $w_t(a_w; X)$, $\sigma_{(NH_4)_{2X}H_{2(1-X)}SO_4}$, and $\rho_{(NH_4)_{2X}H_{2(1-X)}SO_4}$. The Aerosol Inorganics Model (AIM) (Clegg, Brimblecombe, & Wexler, 1998) was employed for $w_t(a_w; X)$. Partitioning of $NH_3$ and $H_2SO_4$ between the condensed and vapor phases, as well as the formation of any solid phases, was omitted. The range of validity of the AIM is limited to water activities above 0.1. Below this value, predictions provided by Clegg and Brimblecombe (1995) were used for $X$ of 0.0. For $X > 0$ but $a_w \leqslant 0.1$, the values of Clegg and Brimblecombe for $w_t(a_w; 0)$ were scaled by the ratio $w_t(0.1; X) : w_t(0.1; 0)$ calculated by the AIM. For $\sigma_{(NH_4)_{2X}H_{2(1-X)}SO_4}$ and $\rho_{(NH_4)_{2X}H_{2(1-X)}SO_4}$, the models of Hyvärinen et al. (2005) and Semmler et al. (2006) were used, respectively. A mole-fraction-weighted equation was used for the density of dry $(NH_4)_{2X}H_{2(1-X)}SO_4$.

We also tested but ruled out hypotheses that nanosize effects on density or surface tension might explain the decreasing growth factors for smaller particles. Gilbert, Huang, Zhang, Waychunas, and Banfield (2004) reported that density increases by ca. 1% below a critical size of 1–5 nm for typical materials. This critical size is smaller than the particle diameters investigated in this work. This fact notwithstanding, the ratio $g^{model}_{bulk}(\mathrm{RH}) : g^{meas}(\mathrm{RH})$ follows from Eqs. (4b) and (5) as proportional to $[\rho_{(NH_4)_2SO_4} : \rho_{H_2SO_4}(w_t(a_w))]^{1/3}$. The disagreement between the model and the measurements therefore decreases in response to a possible nanosize effect that might increase the density of aqueous sulfuric acid nanoparticles. On the other hand, the difference increases in response to a possible increase in the density of ammonium sulfate. Quantitatively, however, even if there were a nanosize effect on density of the larger particles of our study, which would be contrary to the assertion of Gilbert et al., a 1% change would still be insufficient to bring the model into agreement with the measured growth factors. Similar results hold for $g^{model}_{Kelvin}(\mathrm{RH}) : g^{meas}(\mathrm{RH})$. Numerical evaluation of this ratio reveals that the required increases in aqueous density are RH dependent and range from 40% to 190% and 8% to 40% for the particles having theoretical dry diameters of 5.5 and 27.3 nm, respectively (analysis not shown). Such large changes in density are not physically plausible.

Surface tension decreases with decreasing particle diameter, typically below a threshold diameter of a few nm determined by the Tolman length (Lu & Jiang, 2005). Eq. (6) shows that any posited decrease in surface tension would increase $a_w$ for fixed RH. Correspondingly, the hygroscopic growth curve $g^{model}_{Kelvin}(\mathrm{RH})$ would shift left for a decrease in surface tension, thereby increasing the differences between $g^{meas}$ (RH) and $g^{model}_{Kelvin}$ (RH). Agreement between the measurements and the model would require an RH-dependent correction of −85% (at 20% RH) to 200% (at 85% RH) for particles having theoretical dry diameter of 27.3 nm (analysis not shown). The respective changes for 5.5-nm particles would be −75% and 4000%. The magnitudes of these changes are not physically plausible. Furthermore, the supposed negative correction at low RH and positive correction at high RH also suggest that any surface-tension-based explanation would be a fudge factor rather than a systematic physical correction with particle size.

As a final alternative, changes in the particle shape factor were excluded from the analysis because acidified sulfate particles are liquid and hence spherical. Solid ammonium sulfate particles have a shape factor differing by only a small amount from unity (e.g., 0.02, cf. Biskos, Paulsen et al., 2006), and a small uncertainty in $\boldsymbol{d}_{(NH_4)_2SO_4}$ (cf. Eq. (4b)) is insufficient to explain the differences between the model and the observations apparent in Fig. 5.

In summary, measurements of the hygroscopic growth of acidic sulfate particles having theoretical dry diameters from 5.5 to 53.2 nm are reported in this study. The acid content of the particles at low RH (i.e., < 5%) was determined by the size change following $NH_3$ neutralization. The measured hygroscopic growth factors of the largest particles agreed well with the predictions for pure $H_2SO_4/H_2O$ particles. Smaller particles were partially neutralized as $(NH_4)_{2X}H_{2(1-X)}SO_4/H_2O$, and the extent of neutralization monotonically increased both for higher RH conditions and for smaller particles. The atmospheric implication of these results is that the hygroscopic growth factors of newly formed acidic sulfate particles in the atmosphere will be very

sensitive to their extent of neutralization, more so than possible nanosize effects on density and surface tension, arguing for the important effects of simultaneous uptake of $H_2O$ and $NH_3$ for the growth rates and ultimate fate of newly formed particles.

## Acknowledgments

This material is based upon work supported by the National Science Foundation under Grant no. 0304213. We thank John Shilling and Qi Chen for useful discussions and suggestions.

## Appendix A. Supplementary data

Supplementary data associated with this article can be found in the online version at 10.1016/j.jaerosci.2008.12.003.

## References

Biskos, G., Malinowski, A., Russell, L. M., Buseck, P. R., & Martin, S. T. (2006). Nanosize effect on the deliquescence and the efflorescence of sodium chloride particles. *Aerosol Science and Technology*, *40*(2), 97–106.

Biskos, G., Paulsen, D., Russell, L. M., Buseck, P. R., & Martin, S. T. (2006). Prompt deliquescence and efflorescence of aerosol nanoparticles. *Atmospheric Chemistry and Physics*, *6*, 4633–4642.

Biskos, G., Russell, L. M., Buseck, P. R., & Martin, S. T. (2006). Nanosize effect on the hygroscopic growth factor of aerosol particles. *Geophysical Research Letters*, *33*(7), L07801.

Chen, J. P. (1994). Theory of deliquescence and modified Köhler curves. *Journal of Atmospheric Sciences*, *51*(23), 3505–3516.

Clegg, S. L., & Brimblecombe, P. (1995). Application of a multicomponent thermodynamic model to activities and thermal-properties of 0–40 mol $kg^{-1}$ aqueous sulfuric-acid from < 200 to 328 K. *Journal of Chemical and Engineering Data*, *40*(1), 43–64.

Clegg, S. L., Brimblecombe, P., & Wexler, A. S. (1998). Thermodynamic model of the system $H^+$–$NH_4^+$–$Na^+$–$SO_4^{2-}$–$NO_3^-$–$Cl^-$–$H_2O$ at 298.15 K. *Journal of Physical Chemistry*, *102*(12), 2155–2171.

Gilbert, B., Huang, F., Zhang, H., Waychunas, G. A., & Banfield, J. F. (2004). Nanoparticles: Strained and stiff. *Science*, *30*(5684), 651–654.

Gmitro, J. I., & Vermeulen, T. (1964). Vapor–liquid equilibria for aqueous sulfuric acid. *AICHE Journal*, *10*(5), 740–746.

Hyvärinen, A.-P., Raatikainen, T., Laaksonen, A., Viisanen, Y., & Lihavainen, H. (2005). Surface tensions and densities of $H_2SO_4 + NH_3 +$ water solutions. *Geophysical Research Letters*, *32*(16), L16806.

Jackervoirol, A., & Mirabel, P. (1989). Heteromolecular nucleation in the sulfuric acid–water system. *Atmospheric Environment*, *23*(9), 2053–2057.

Kim, J. H., Mulholland, G. W., Kukuck, S. R., & Pui, D. Y. H. (2005). Slip correction measurements of certified PSL nanoparticles using a nanometer differential mobility analyzer (nano-DMA) for Knudsen number from 0.5 to 83. *Journal of Research of the National Institute of Standards and Technology*, *110*(1), 31–54.

Kulmala, M., Laaksonen, A., & Pirjola, L. (1998). Parameterizations for sulfuric acid/water nucleation rates. *Journal of Geophysical Research—Atmospheres*, *103*(D7), 8301–8307.

Kulmala, M., Riipinen, I., Sipila, M., Manninen, H. E., Petaja, T., Junninen, H. et al. (2007). Toward direct measurement of atmospheric nucleation. *Science*, *318*(5847), 89–92.

Leaderer, B. P., Naeher, L., Jankun, T., Balenger, K., Holford, T. R., Toth, C. et al. (1999). Indoor, outdoor, and regional summer and winter concentrations of $PM_{10}$, $PM_{2.5}$, $SO_4^{2-}$, $H^+$, $NH_4^+$, $NO_3^-$, $NH_3$, and nitrous acid in homes with and without kerosene space heaters. *Environmental Health Perspectives*, *107*(3), 223–231.

Lu, H. M., & Jiang, Q. (2005). Size-dependent surface tension and Tolman's length of droplets. *Langmuir*, *21*(2), 779–781.

Martin, S. T. (2000). Phase transitions of aqueous atmospheric particles. *Chemical Reviews*, *100*, 3403–3453.

McMurry, P. H., Takano, H., & Anderson, G. R. (1983). Study of the ammonia (gas) sulfuric-acid (aerosol) reaction-rate. *Environmental Science and Technology*, *17*(6), 347–352.

Middlebrook, A. M., Thomson, D. S., & Murphy, D. M. (1997). On the purity of laboratory-generated sulfuric acid droplets and ambient particles studied by laser mass spectrometry. *Aerosol Science and Technology*, *27*(3), 293–307.

Mudd, H. T., Kruger, C. H., & Murray, E. R. (1982). Measurement of IR laser backscatter spectra from sulfuric acid and ammonium sulfate aerosols. *Applied Optics*, *21*(6), 1146–1154.

Pirjola, L., & Kulmala, M. (1998). Modelling the formation of $H_2SO_4$–$H_2O$ particles in rural, urban and marine conditions. *Atmospheric Research*, *46*(3–4), 321–347.

Rader, D. J., & McMurry, P. H. (1986). Application of the tandem differential mobility analyzer to studies of droplet growth or evaporation. *Journal of Aerosol Science*, *17*(5), 771–787.

Sarangapani, R., & Wexler, A. S. (1996). Growth and neutralization of sulfate aerosols in human airways. *Journal of Applied Physiology*, *81*(1), 480–490.

Seinfeld, J. H., & Pandis, S. N. (1998). *Atmospheric chemistry and physics: From air pollution to climate change*. New York: Wiley.

Semmler, M., Luo, B. P., & Koop, T. (2006). Densities of liquid $H^+/NH_4^+/SO_4^{2-}/NO_3^-$/H2O solutions at tropospheric temperatures. *Atmospheric Environment*, *40*(3), 467–483.

Suh, H. H., Koutrakis, P., & Spengler, J. D. (1994). The relationship between airborne acidity and ammonia in indoor environments. *Journal of Exposure Analysis and Environmental Epidemiology*, *4*(1), 1–22.

Weber, R. J., Marti, J. J., McMurry, P. H., Eisele, F. L., Tanner, D. J., & Jefferson, A. (1996). Measured atmospheric new particle formation rates: Implications for nucleation mechanisms. *Chemical Engineering Communications*, *151*(53–54), 53–64.

Weber, R. J., McMurry, P. H., Mauldin, R. L., Tanner, D. J., Eisele, F. L., Clarke, A. D. et al. (1999). New particle formation in the remote troposphere: A comparison of observations at various sites. *Geophysical Research Letters*, *26*(3), 307–310.

Xiong, J. Q., Zhong, M. H., Fang, C. P., Chen, L. C., & Lippmann, M. (1998). Influence of organic films on the hygroscopicity of ultrafine sulfuric acid aerosol. *Environmental Science and Technology*, *32*(22), 3536–3541.

Yu, F. Q., & Turco, R. P. (2001). From molecular clusters to nanoparticles: Role of ambient ionization in tropospheric aerosol formation. *Journal of Geophysical Research—Atmospheres*, *106*(D5), 4797–4814.

Zhang, Q., Stanier, C. O., Canagaratna, M. R., Jayner, J. T., Wornsnop, D. R., Pandis, S. N. et al. (2004). Insights into the chemistry of new particle formation and growth events in Pittsburgh based on aerosol mass spectrometry. *Environmental Science and Technology*, *38*(18), 4797–4809.